Amphiphilic DNA and its application in biomedicine

Li, Hongyan

DOI:
10.33612/diss.125274906

3

Fast, Efficient, and Targeted Liposome Delivery Mediated by DNA

Parts of this chapter were published in: Adv. Healthc. Mater. 2019, 1900389.

3.1 Introduction

Many exogenous compounds, e.g., disease related therapeutic drugs,[1, 2, 3] metabolites,[4, 5] or imaging agents,[6, 7] are solely functional in vitro or in vivo once effectively delivered to the interior of cells in adequate amounts. Hence, insufficient cellular accumulation often is a criterion for exclusion of drugs for biological and therapeutic applications. Generally, the delivery pathway is predetermined by the drug's physicochemical properties. This implies that hydrophilic drugs are usually prevented from entering cells freely due to the lipophilic character of cellular membrane[8] and most proteins cannot diffuse into the cell owed to their large hydrodynamic radius.[9] In addition to insufficient delivery, free drugs also possess undesired systemic side effects when they distribute freely throughout the body.[10] One method to circumvent these limitations is to load drugs into nanosized carriers to facilitate their transport to the desired site with high efficiency by the enhanced permeability and retention (EPR) effect.[10] In this regard, liposomes are the most frequently investigated nanocarrier due to their biocompatibility, ability for self-assembly, high drug loading capacity, and a wide range of physicochemical and biophysical properties that can be tailored to control their pharmacological characteristics.[11] Targeting ligands, e.g., small molecules such as folic acid,[12, 13, 14] antibodies,[15, 16] or DNA aptamers,[17, 18] can be conjugated to liposomes to further facilitate their cellular recognition and uptake capabilities. Most notably, neutral liposomes were elegantly designed for enhanced cellular uptake by anchoring coiled-coil peptides that locally trap the liposome in the vicinity of the cell membrane eventually releasing cargo upon internalization with high affinity.[19] However, this approach is inherently limited by its low recognition selectivity based on the nonspecific coiled-coil peptide interactions. Moreover, their chemical and physical instability further impedes the application of peptides in drug delivery. Biomacromolecular DNA outperforms peptides in these aspects, as it is programmable based on Watson–Crick base pairing and chemical modifications allow endowing it with notably high biological stability. Amphiphilic lipid DNA consists of DNA conjugated to a hydrophobic motif, either a small molecule such as cholesterol,[20] long hydrocarbon lipids,[21] or polymers.[22] These lipid DNA strands can be anchored to membranes, thus rendering their application in

cellular surface engineering,[23] drug delivery,[24] cellular dynamic event detection,[25, 26] and cell assembly[21, 27] possible.

Based on the high specificity and membrane insertion capability of lipid DNA, we here report a new and efficient targeted liposome delivery method mediated by DNA hybridization recognition (**Fig. 3.1**). Two complementary single DNA strands were anchored on either the cellular or the liposomal membrane. Hybridization between these two strands locally trapped liposomes and cells in each other's vicinity, enabling the internalization and delivery of the cargo.

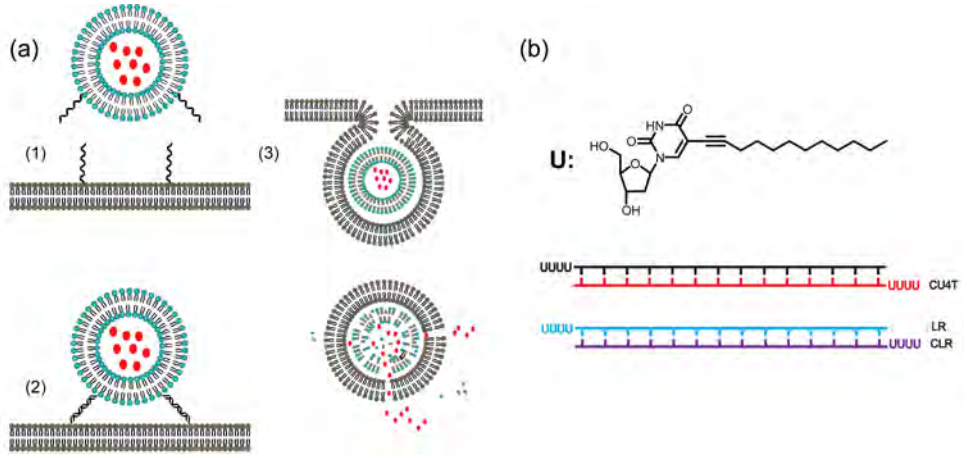

Figure 3.1 | (a) Schematic illustration of cellular liposome internalization by DNA hybridization. (1) Liposome and cell are approaching each other; (2) Liposome is tethered to cell membrane by DNA hybridization of complementary strands; (3) Cellular endocytosis trafficking and liposome cargo (red dots) diffusion. (b) Schematic illustration of DNA strands used in this chapter. **U** represents dodecyne modified deoxyuridine nucleotide.

3.2 Results and Discussions

3.2.1 Enhanced Cellular Uptake by DNA Hybridization

As lipid DNA could be stably and accessibly grafted to both liposomal and cellular membrane as seen from **Chapter 2**, we were intrigued whether these DNA anchors could be exploited to steer the cellular internalization process once hybridized with the complementary DNA on a carrier liposome surface. To investigate this, cells pre-anchored with CU4T were incubated for 15 min with U4T-modified

liposomes labeled with 1% NBD-DHPE. Notably, CLSM (**Fig. 3.2a**) reveals significant internalization of the liposome, whereas U4T-modified liposomes incubated with non-complementary U4T-grafted cells, or non-modified liposome incubated with non-modified cells, did not show detectable cellular uptake. This suggests hybridization-promoted cellular uptake of liposomes. Further flow cytometric measurements (**Fig. 3.2b**) corresponded well with this enhanced uptake and analysis of the median fluorescence of the liposomes demonstrated 18 times higher uptake as compared with the non-hybridized control(**Fig. 3.2c**).

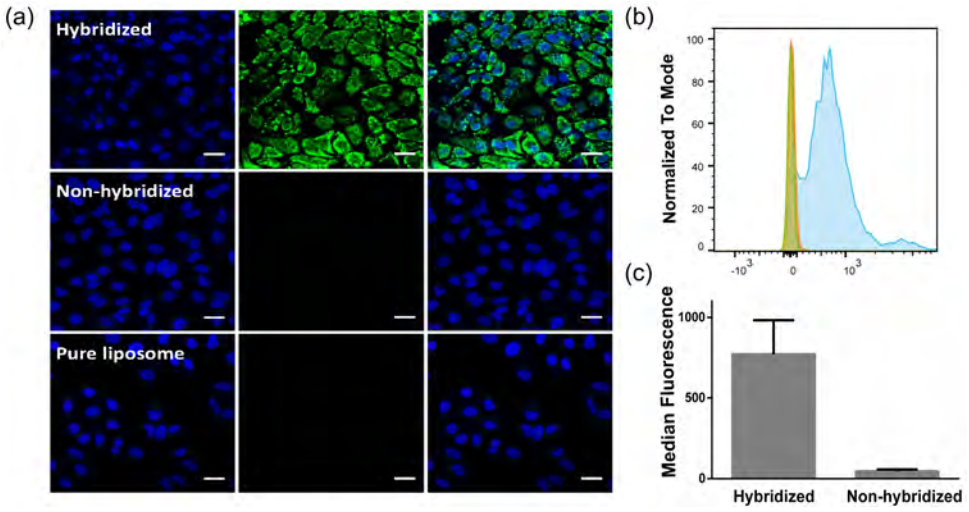

Figure 3.2 | Demonstration of enhanced liposome delivery by DNA hybridization. Liposome composition: DOPC:DOPE:NBD-DHPE:cholesterol = 2:1:0.03:1. Hybridized: cell surface equipped with CU4T, liposome surface anchored with U4T; Non-hybridized: cell surface anchored with U4T, liposome surface anchored with U4T; Pure liposome: neither cell nor liposome surfaces were anchored with lipid DNA. (a) Enhanced liposome delivery visualized by CLSM. Blue: Hoechst 33342; Green: NBD. Scale bar: 50 μm. (b) Enhanced liposome delivery by flow cytometry. Blue: hybridized; Red: non-hybridized; Orange: pure liposome; Green: untreated cell. (c) Comparison of median fluorescence intensity of internalized NBD liposomes. Error bars indicate SD from the mean (n = 3).

To elucidate the uptake mechanism, we encapsulated two water-soluble dyes, calcein and propidium iodide (PI), into the liposomes showing fast and enhanced intercellular uptake (**Fig. 3.12**). Subsequently, to reveal uptake kinetics, a time-dependent examination was performed. After anchoring with CU4T, cells were incubated with U4T liposomes and investigated at different time points. Liposome uptake started after 2 min and with increasing incubation time, larger quantities

of liposomes were internalized, whereas non-hybridized liposome controls did not show any visible uptake even after 30 min (**Fig. 3.3**).

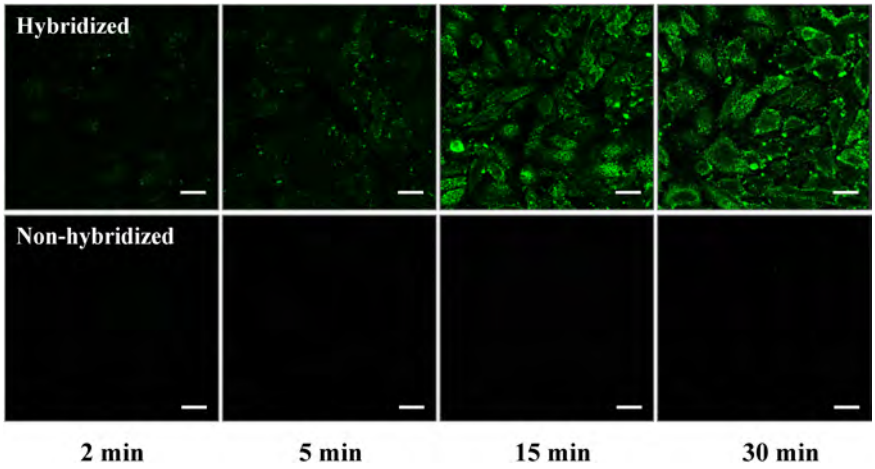

Figure 3.3 | CLSM micrographs of liposome (DOPC:DOPE:NBD-DHPE:cholesterol = 2:1:0.03:1) internalization by cells at 2 min, 5 min, 15 min, and 30 min. Hybridized: cell surface anchored with CU4T, liposome surface anchored with U4T; Non-hybridized: cell surface anchored with U4T, liposome surface anchored with U4T. Green: NBD. Scale bar: 50 μm.

3.2.2 Specific Delivery by DNA Hybridization

Having confirmed that DNA hybridization could promote cellular uptake of the liposomes, the propensity for this mechanism to succeed in a more complex environment was explored. Therefore, cells were separately seeded in a bottomless chamber fixed to a Petri dish bottom and incubated with either U4T or LR. Then, the chamber was removed and all cells were exposed to a mixture of U4T-anchored NBD liposome and LR-anchored ATTO655 liposomes, resulting in the successful delivery of different liposomes to different cell populations (**Fig. 3.4**).

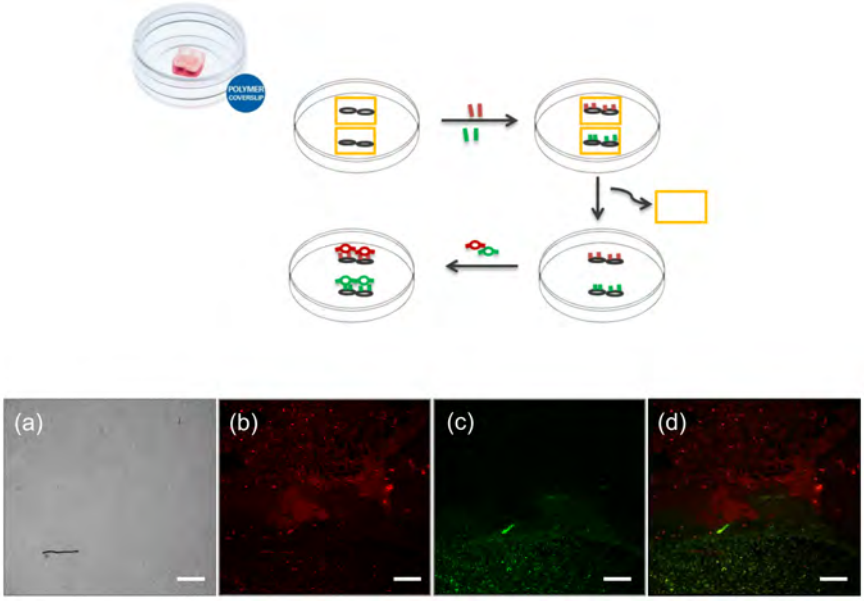

Figure 3.4 | Dual targeting of liposome to adherent cells. Top: schematic illustration of experiments. Bottom: CLSM micrographs of cells after dual targeting with liposome. Cells treated with U4T and LR were incubated with a mixed NBD liposome (DOPC:DOPE:NBD-DHPE:cholesterol = 2:1:0.03:1) solution and ATTO655 liposome (DOPC:DOPE:ATTO655-DOPE:cholesterol = 2:1:0.03:1) solution. (a) Brightfield image shows two separated cell populations; (b) ATTO655; (c) NBD; (d) Overlay of ATTO655 and NBD. Scale bar: 500 μm.

To additionally prove the working concept in cell suspensions, two populations of trypsinized cells were employed. One population was pre-anchored with CU4T, while the other population was pre-anchored with LR and stained with Hoechst 33342. After sufficient washing, the two cell populations were mixed. Liposomes pre-anchored with U4T were incubated with this mixed cell population. By specific recognition of U4T with CU4T, liposomes only docked on CU4T cells, but not on LR-grafted cells (**Fig. 3.5a, b**). Even more challenging, a mixed liposome solution with either U4T or LR was incubated with mixed cell populations bearing either CU4T or CLR (stained with Hoechst 33342). Notably, the assigned liposomes docked on the targeted cell surfaces (**Fig. 3.5c, d**).

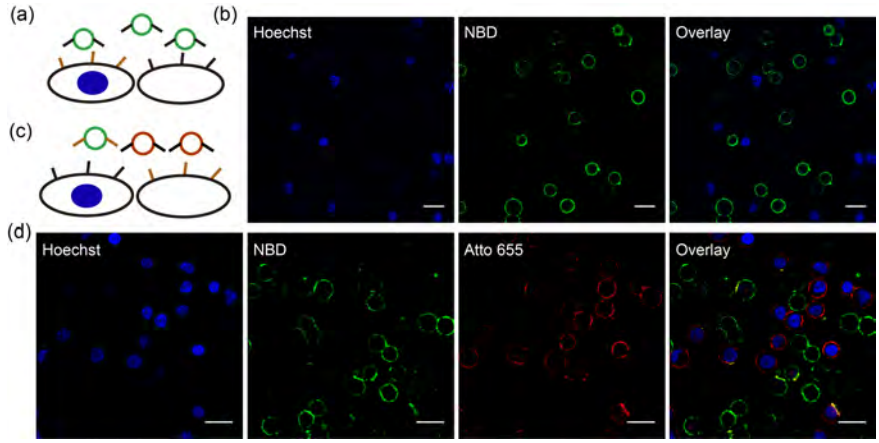

Figure 3.5 | CLSM micrographs of targeted delivery of liposomes to cells. (a) Schematic illustration of single liposome population delivery. (b) CLSM images of single liposome population delivery. Liposomes (DOPC:DOPE:NBD-DHPE:cholesterol = 2:1:0.03:1) anchored with U4T were incubated with a mixed cell population anchored with CU4T or LR (labeled with Hoechst 33342). Blue: Hoechst 33342; Green: NBD. (c) Schematic illustration of dual liposome population delivery. (d) CLSM images of dual liposome population delivery. U4T anchored liposomes (DOPC:DOPE:NBD-DHPE:cholesterol = 2:1:0.03:1) and LR anchored liposome (DOPC:DOPE:ATTO655-DOPE:cholesterol = 2:1:0.03:1) were incubated with a mixed cell population anchored with CU4T or CLR (labeled with Hoechst 33342). Blue: Hoechst 33342; Green: NBD; Red: ATTO655. Scale bar: 25 μm.

3.2.3 Mechanism of Liposome Cellular Uptake

Generally, internalization of nanostructures proceeds via membrane fusion, macropinocytosis, or receptor-mediated endocytosis. However, the punctuate intercellular distribution we observe for our liposomes (**Fig. 3.2a**) differs considerably from the liposome cell fusion mechanism suggested for a comparable lipid DNA-based system that was developed simultaneously to our work.[28] By applying various conditions and inhibitors, we thus strived to exclude certain uptake pathways and shine light on the prevalent internalization mode. We excluded uptake via membrane fusion by performing low temperature internalization inhibition experiments, since fusion processes are widely temperature independent.[28, 29, 30] For this purpose, cells anchored with CU4T were ice-cooled and then incubated with U4T liposomes for 15 min in the cold. NBD fluorescence from the liposomes was found mainly on the cell membrane (**Fig. 3.6**) hinting towards a largely energy-dependent active uptake process, as opposed to the passive fusion uptake.

Furthermore, the extent of macropinocytosis was evaluated by incubating cells with the macropinocytosis marker rhodamine B-dextran 70 kDa and negligible signal was detected (**Fig. 3.13**), suggesting a minor contribution of macropinocytosis in liposome uptake via the DNA hybridization process.

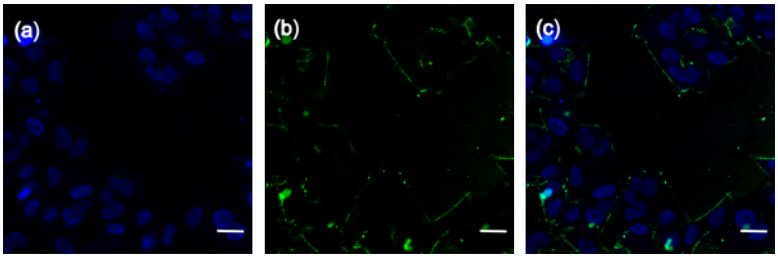

Figure 3.6 | CLSM micrographs of cellular uptake of liposome (DOPC:DOPE:NBD-DHPE:cholesterol = 2:1:0.03:1) at low temperature. (a) Hoechst 33342; (b) NBD; (c) Overly of Hoechst 33342 and NBD. Scale bar: 25 μm.

Since membrane fusion and macropinocytosis were excluded, it was likely that cells internalized liposomes by receptor-mediated endocytosis. Two well-studied examples for this are clathrin- and caveolae-dependent endocytosis (**Fig. 3.7**). The clathrin-dependent pathway is initiated when clathrin, together with other cytosolic proteins, cluster on the inner leaflet of the plasma membrane. This results in a 'clathrin-coated pit'. After detachment and uncoating, cargo-filled vesicles traffic further within the cell.[31] Concomitantly, caveolae are flask-shaped membrane invaginations. Upon binding with specific ligands, caveolae can bud from the membrane and are internalized.[32],[33] Both clathrin- and caveolae-dependent endocytosis can be inhibited by their corresponding chemical inhibitors. Chlorpromazine was established to block clathrin-dependent endocytosis by translocating clathrin and its adaptor protein from the cell surface to the endosomes.[34] Alongside, methyl-β-cyclodextrin was reported to remove cholesterol essential for caveolae formation out of the plasma membrane thus inhibiting caveolae-dependent endocytosis.[35] Moreover, cell surface receptor scavengers were reported to mediate endocytosis of oligonucleotide modified gold nanoparticles[36, 37] or DNA nanostructures,[38] which can be inhibited by polyinosinic acid (poly I) competitively binding these scavenger receptors. To determine which endocytosis pathway was involved in this DNA hybridization induced uptake and

whether scavenger receptors play a role, differences in liposome uptake efficiency after cell treatment with the corresponding inhibitors were examined. Therefore, cells were first grafted with CU4T, then incubated with different inhibitors, followed by incubation with NBD-labelled liposomes in the presence of inhibitors. The resulting NBD fluorescence intensity was quantified by flow cytometry and displayed as signal normalized to untreated controls (**Fig. 3.8**). It clearly shows that treatment with methyl-β-cyclodextrin greatly decreased the liposome uptake, indicating that caveolae-mediated endocytosis was the dominant liposome internalization pathway. Poly I inhibition reduced liposome uptake, suggesting that HeLa cells rely on scavenger receptors to internalize oligonucleotide-modified liposomes.

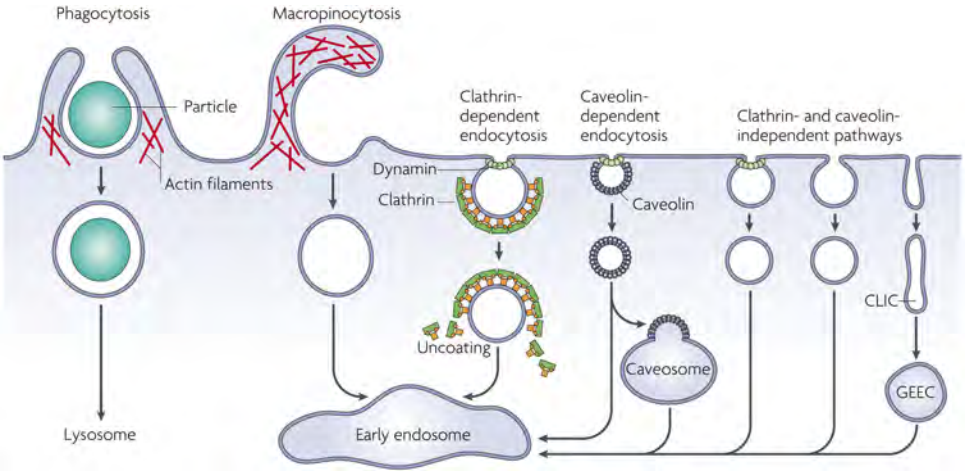

Figure 3.7 | Pathways of entry into cells.[33] Substances can enter cells by phagocytosis, macropinocytosis, clathrin-dependent endocytosis, caveolin-dependent endocytosis and clathrin- or caveolin- independent pathways.

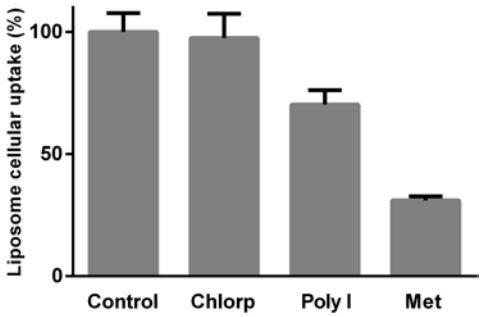

Figure 3.8 | Cellular liposome internalization efficiency after treatment with different inhibitors. CU4T anchored cells were pretreated with inhibitors for 15 min before incubation with U4T-anchored liposome (DOPC:DOPE:NBD-DHPE:cholesterol = 2:1:0.03:1) in inhibitor solutions. Percentage of median fluorescence intensity of internalized liposome is displayed. Control: untreated cell; Chlorp: cells pretreated with 200 μM chlorpromazine; Poly I: cells pretreated with 50 μg·mL^{-1} poly I. Met: cells pretreated with 12.5 mg·mL^{-1} methyl-β-cyclodextrin. Error bars indicate SD from the mean (n = 3).

3.2.4 After Endocytosis

To characterize liposome cargo fate after caveolae-mediated endocytosis, the liposome membrane was labeled with a fluorescent lipid (Marina Blue-DHPE) and the aqueous core was labeled with a hydrophilic cargo dye (calcein) at a self-quenching concentration visualizing liposomal integrity and cargo release after internalization. The delivery location depends on its respective polarity and hence solubility of the cargo molecule. While we expected hydrophobic Marina Blue-DHPE to be delivered via the hydrophobic regions of the cell, e.g. lysosome membrane, we hypothesized that hydrophilic calcein would be released into the hydrophilic regions of the cell, e.g. lysosome lumen or cytosol. Additionally, cellular lysosomes were stained by Lyso-tracker Red, since most endocytosis events co-locate with the lysosome. CLSM (**Fig. 3.9**) clearly showed that after 15 min uptake, the majority of Marina Blue overlaid with calcein, indicative of intact liposomes in this timeframe. In addition, there was no evidence of co-localization of liposomes with the lysosome. Most probably at this time point, the liposomes were located in the endocytic vesicles. After 2 h incubation, minor separation of Marina Blue and calcein signals suggested beginning disassembly of the liposomes. Additionally, a considerable overlap of the liposomes and lysosome was

identified, suggesting that the liposomes had reached the lysosome at this point. After 4 h incubation, self-quenched calcein was evenly distributed within the cytosol with a brighter signal while Marina Blue was still located in the lysosome.

All the above results suggest the following mechanism for uptake and fate of the liposomes: when the liposomes get in contact with the cell membrane, they attach by hybridization through Watson-Crick base pairing between complementary strands anchored on the cell- and on the liposome surface. Upon residing on the cell membrane, the liposomes are taken up by the cells via a caveolae-mediated endocytic pathway. Once reaching the lysosome, the liposomes disassemble and their cargo is released.

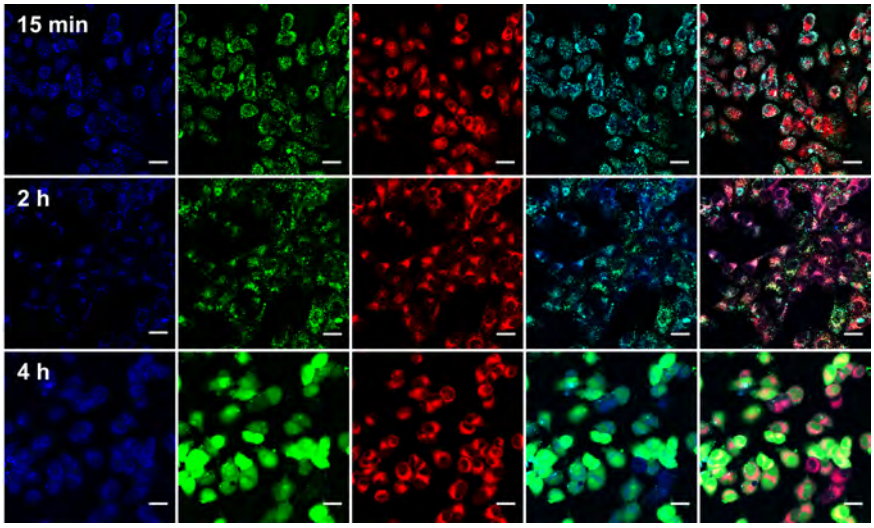

Figure 3.9 | CLSM micrographs of liposome delivery after different time points. U4T anchored liposome (DOPC:DOPE:Marine Blue-DHPE:cholesterol = 2:1:0.03:1) was loaded with calcein then incubated with CU4T anchored cells for 15 min, 2 h, and 4 h. Afterwards, lysosomes were stained with Lyso-Tracker Red. Blue: Marine Blue; Green: calcein; Red: Lyso-Tracker Red. Scale bar: 50 μm.

3.2.5 Cellular Toxicity

High cell viability and regular proliferative capacity are prerequisites for a successful cargo delivery system and hence cellular toxicity tests were performed on cells treated with CU4T and the complementary U4T liposomes. The results indicated that cell viability after treatment was acceptable (**Fig. 3.10**).

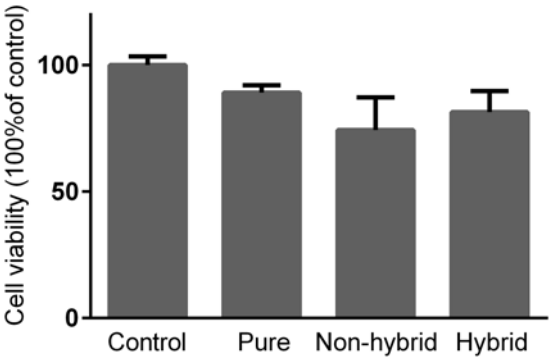

Figure 3.10 | Cell viability of liposome delivery system. Control: untreated cell; Pure: neither cell nor liposome surfaces were anchored with lipid DNA. Non-hybrid: cell surface anchored with U4T, liposome surface anchored with U4T; Hybrid: cell surface anchored with CU4T, liposome surface anchored with U4T. Error bars indicate SD of the mean (n = 3).

3.3 Conclusion

Here, we employed artificial DNA receptors as recognition motifs to target, locally trap, and thus enrich lipid DNA-grafted liposomes in the vicinity of cells functionalized with the complementary lipid DNA strand. By CLSM and flow cytometric measurements, we demonstrated that the principle working mechanism of this technique was neither caused by nonspecific cellular adsorption nor internalization, but only by DNA hybridization. Most notably, we demonstrated selective addressability of specific cells with specific liposomes in a complex cell-liposome population highlighting the intrinsic advantages of DNA-hybridization over other targeting techniques reported in the literatures.[13, 29, 39] Various fluorescent marker molecules were loaded as drug model compounds to these liposomes and their uptake pathways and kinetics were investigated. Thoroughly analyzing the uptake pathway by varying uptake conditions and applying inhibitors, we elucidated that cells internalized liposomes most efficiently by caveolae-dependent endocytosis. This result is in stark contrast to a system developed in parallel to our work, where a comparable lipid DNA recognition motif was found to promote liposome-cell fusion instead.[28] The authors of this work rely on cholesterol units tethered to the DNA with a hydrophilic tetraethylene glycol spacer. We hypothesize that the cholesterol units destabilize the lipid bilayer and the

hydrophilic spacer increases binding flexibility, both facilitating a fusion process.[40] In contrast, our liposomes anchored with aliphatic chains conjugated directly to the DNA might be more stable and rigid, hence favoring the endocytic pathway. As liposomes delivered their cargo mainly to the lysosome, we believe that this release system is a promising candidate for the targeted treatment of lysosome-related diseases,[41] such as metabolic illnesses and lysosome storage disorders.[42] Moreover, this delivery mechanism enhanced by DNA hybridization can be expanded towards more complex structures, e.g. nanoparticles or DNA nanostructures.[43, 44]

3.4 Experimental Section

3.4.1 Materials

All chemicals and reagents purchased from commercial suppliers were used without further purification unless noted. ATTO655-DOPE was purchased from ATTO-TEC. Calcein, Triton X-100, chlorpromazine, methyl-β-cyclodextrin, and polyinosinic acid were purchased from Sigma Aldrich. Propidium iodide was from BioLegend. Phenol red free DMEM, Hoechst 33342, LysoTracker® Red DND-99, Alexa 647-transferrin from human serum, Alexa 647-Cholera toxin subunit B, and Rhodamine B-neutral dextran 70k MW were acquired from Thermo Fisher Scientific. Culture-insert 2 well chamber frame were purchased from ibidi. All oligonucleotides without lipid modification were purchased from biomers.

3.4.2 DNA Used

Lipid DNA was synthesized as described in **Chapter 2** and the successful synthesis was confirmed by MALDI-TOF mass spectrometry (**Fig. 3.11**). Sequences of used lipid DNA in this chapter are listed in **Table 3.1**.

Name	Sequence (5' to 3')
U4T18	**UUUU**GCGGATTCGTCTGC
CU4T	**UUUU**GCGGATTCGTCTGC
LR	**UUUU**ACCACCTACATCAC
CLR	**UUUU**GTGATGTAGGTGGT

Table 3.1 | Sequences of lipid DNA in this chapter.

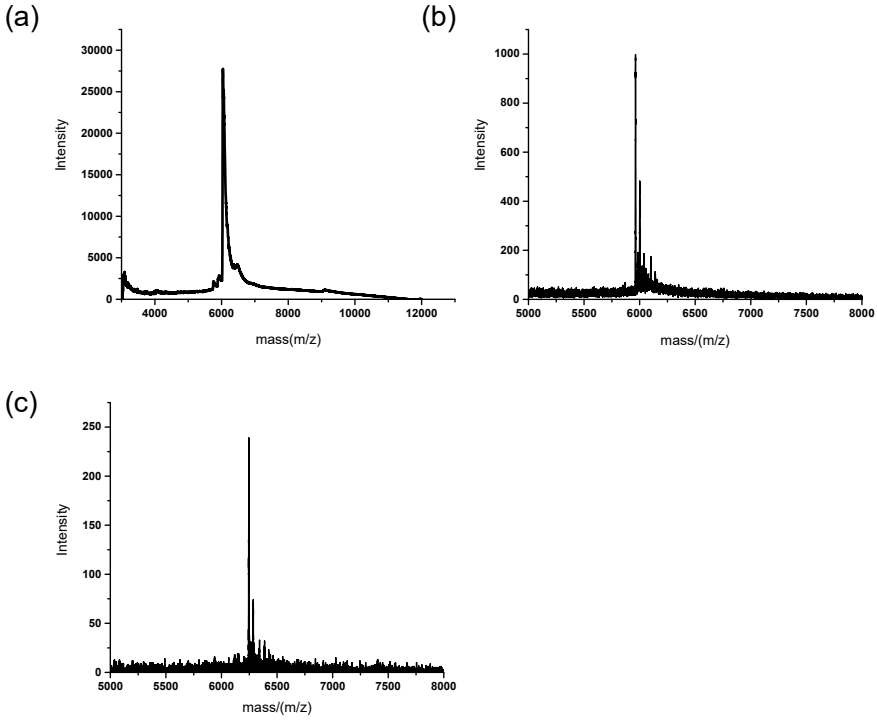

Figure 3.11 | MALDI-TOF mass spectra of lipid-DNA used in the experiments. (a) CU4T (calcd.: 6020 g·mol^{-1}, found: 6082 g·mol^{-1}), (b) LR (calcd.: 5900 g·mol^{-1}, found: 6022 g·mol^{-1}) and (c) CLR (calcd.: 6153 g·mol^{-1}, found: 6245 g·mol^{-1}).

3.4.3 Confocal Microscopy Sample Preparation

For enhanced NBD liposome uptake, HeLa cells ($2{\cdot}10^5$ mL^{-1}, 300 μL) were seeded at μ-Slide 8 well for overnight culture. Then incubated with CU4T (10 μM) for 20 min and followed with 15 min incubation with NBD labelled liposome (0.8 mM) pre-anchored with U4T. Before taking images, cells were stained with Hoechst 33342 (5 $\mu g{\cdot}mL^{-1}$) in phenol red free DMEM for 20 min.

For single targeting experiments in the suspension cell, HeLa cells were detached and incubated in serum free DMEM with either CU4T (10 μM) or LR (10 μM) with $4{\cdot}10^5$ mL^{-1} densities for 20 min. After rinsing with PBS, LR cells were incubated with Hoechst 33342 in culture medium for 20 min while CU4T cells were not. After washing, the two cell populations were mixed and incubated for 15 min with NBD liposomes pre-anchored with U4T.

For dual targeting experiments in the suspension cell, detached cells were incubated in serum free DMEM medium with either CU4T (10 μM) or CLR (10 μM) with $4{\cdot}10^5$ mL^{-1} densities for 20 min. After rinsing with PBS, LR cells were incubated with Hoechst 33342 in culture medium for 20 min while CU4T cells did not. After washing, the two cell populations were combined and incubated for 15 min with a mixer of NBD liposomes (DOPC:DOPE:NBD-DHPE:cholesterol = 2:1:0.03:1) pre-anchored with U4T and ATTO655 liposomes (DOPC:DOPE:ATTO655-DOPE:cholesterol = 2:1:0.03:1) anchored with LR.

For calcein delivery experiments, cellular incubation with CU4T was the same as described above. Then calcein (80 mM) loaded and U4T anchored liposome solution (1% Marina Blue-DHPE incorporated) were incubated with cells for 15 min, 2 h, and 4 h, respectively. After culturing, cells were rinsed with PBS for several times and further incubated with Lyso-Tracker Red (100 nM) for 30 min followed by another washing step. Then fresh phenol red free DMEM was introduced before imaging.

3.4.4 Flow Cytometry Measurements

For enhanced NBD liposome uptake, 500 μL HeLa cells ($6{\cdot}10^5$) were incubated with 10 μM CU4T for 20 min, then NBD labelled liposome (0.8 mM) pre-anchored with U4T were added for 15 min incubation. After PBS rinsing, cells were measured.

For endocytosis inhibitor treatments, 500 μL cells ($6{\cdot}10^5$) pre-anchored with CU4T were incubated in culture medium with endocytosis inhibitor chlorpromazine (40 μM) or methyl-β-cyclodextrin (12.5 mg$\cdot$mL^{-1}) for 15 min. After rinsing, cells were suspended in new culture medium containing corresponding inhibitor, then U4T anchored liposomes were added and incubated with cells for further 15 min. After several times washing with PBS buffer, cells were measured. Flow cytometry measurement data were presented as median $\pm$ standard deviation (n = 3).

3.4.5 Uptake of Calcein and PI Loaded Liposomes

Liposome lipids and U4T dry layer were rehydrated with calcein (80 mM) or PI (1.5 mM) in PBS. After encapsulation, free calcein or PI were removed from liposome solution by PD-10 column and stored at 4 °C before use. HeLa cells were incubated with CU4T for 20 min, then calcein or PI loaded U4T liposome were added for 15 min incubation. After rinse and staining with Hoechst 33342, cells were imaged by confocal microscopy.

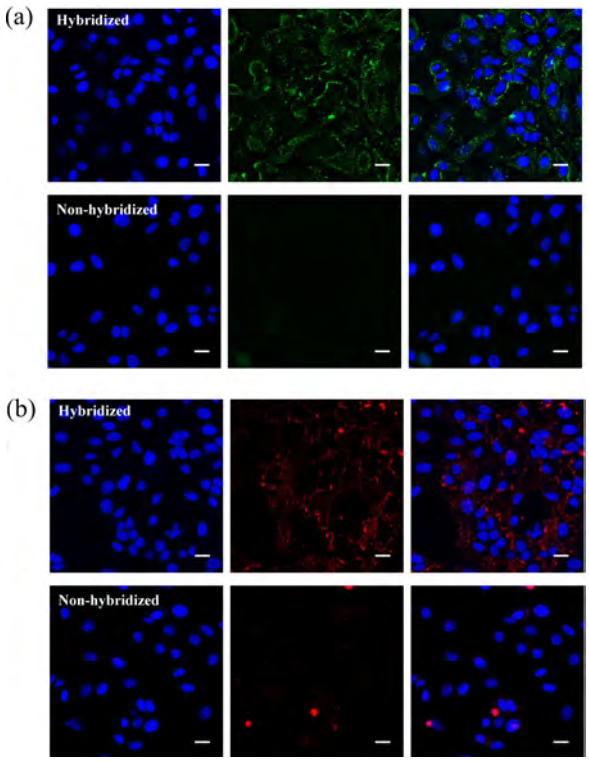

Figure 3.12 | CLSM micrographs of enhanced uptake of calcein and PI loaded liposome. Hybridized: cell surface anchored with CU4T, liposome surface anchored with U4T; Non-hybridized: cell surface anchored with U4T, liposome surface anchored with U4T. (a) Uptake of calcein loaded liposome. Blue: Hoechst 33342, green: calcein. (b) Uptake of PI loaded liposome. Blue: Hoechst 33342, red: PI. Scale bar: 50 μm.

3.4.6 Proliferation Assay

HeLa cells were seeded at a density of 10^4 per well in triplicate in 96 well plates and grown over night at 37 °C, 5% CO_2. Either U4T or CU4T in serum free DMEM were added and incubated for 20 min; afterwards U4T modified liposomes in serum free medium were added and further incubated for 15 min. After washing, new complete DMEM media was introduced for further 24 h culturing. Then cell viability was determined by XTT as recommended by the manufacturer ATCC. Data were presented as mean ± standard deviation (n = 3).

3.4.7 Specific Delivery

For dual targeting experiments of adherent cells, cells were separately seeded in culture insert 2 well chamber fixed at a bottom of a Petri dish. After overnight culture, U4T (10 μM) or LR (10 μM) in culture medium were incubated with cells in different chambers for 20 min. After washing several times, the chamber frame was removed and a mixer of NBD liposome pre-anchored with U4T and ATTO655 liposome pre-anchored with LR were incubated with cells for 15 min. After several washing steps, cells were imaged.

3.4.8 Liposome Uptake at Low Temperature

To study the effect of temperature on cellular uptake of liposomes, cells pre-anchored with CU4T were put on ice for 1 h, and then new medium with NBD labelled liposome pre-anchored with U4T was added and incubated on ice for 15 min, then stained with Hoechst 33342 on ice and sufficiently rinsed with cold PBS before confocal imaging.

3.4.9 Macropinocytosis of HeLa Cells

Macropinocytosis of HeLa cells was demonstrated with macropinocytosis marker rhodamine B-dextran (70 kDa). Cells were seeded overnight and incubated with rhodamine B-dextran 70 kDa (1 mg·mL^{-1}) for 15 min. After sufficient rinsing, cells were imaged under confocal microscopy.

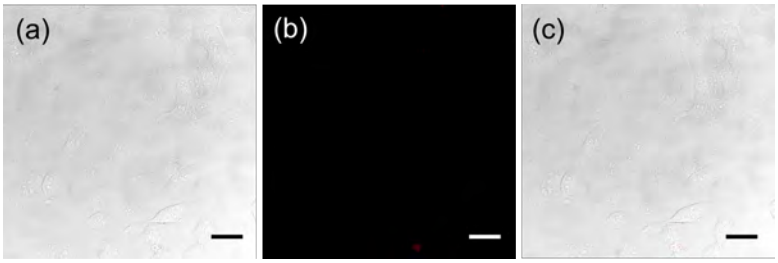

Figure 3.13 | CLSM micrographs of cellular uptake of rhodamine B-dextran (70 kDa). (a) Brightfield; (b) Rhodamine B; (c) Overlay; Scale bar: 50 μm.

3.4.10 Proof of Endocytosis Inhibition

To prove endocytosis inhibitors that do block certain endocytosis pathways, specific endocytosis markers were used. Cells pre-anchored with CU4T were incubated with culture medium containing 200 μM chlorpromazine or 12.5 mg·mL^{-1} methyl-β-cyclodextrin for 15 min. After rinsing, Alexa 647-transferrin (25 μg·mL^{-1}) in 200 μM chlorpromazine or Alexa 647-cholera toxin subunit B (5 μg·mL^{-1}) in 12.5 mg·mL^{-1} methyl-β-cyclodextrin were added and incubated with cells for further 15 min. Then the medium was removed and 300 μL new medium with inhibitors were added for imaging.

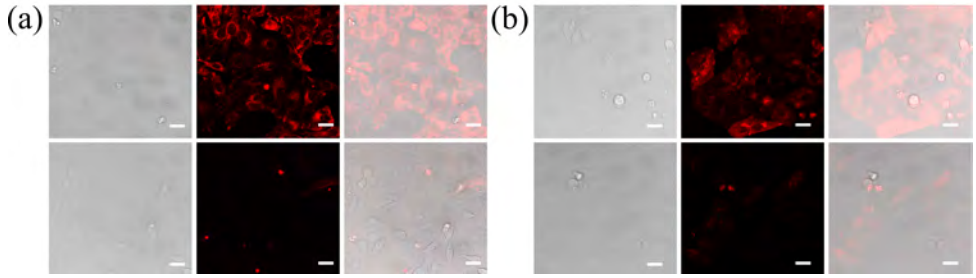

Figure 3.14 | CLSM micrographs of transferrin and cholera toxin subunit B cellular uptake. (a) Transferrin uptake. Top: transferrin uptake after cells were incubated with only medium. Bottom: transferrin uptake after cells were treated with 200 μM chlorpromazine. (b) Cholera toxin subunit B uptake. Top: cholera toxin subunit B uptake after cells were incubated with only medium. Bottom: cholera toxin subunit B uptake after cells were treated with 12.5 mg ·mL^{-1} methyl-β-cyclodextrin. Scale bar: 50 μm.

Bibliography

[1] B. Rothbard, P. A. Khavari, S. Garlington, Q. Lin, T. Kirschberg, E. Kreider, P. L. McGrane, P. A. Wender, Nat. Med. 2000, 6, 1253.

[2] N. Nasongkla, X. Shuai, H. Ai, B. D. Weinberg, J. Pink, D. A. Boothman, J. Gao, Angew. Chem. 2004, 116, 6483;

[3] T. Feng, X. Ai, G. An, P. Yang, Y. Zhao, ACS Nano. 2016, 10, 4410.

[4] D. H. Han, H.-K. Na, W. H. Choi, J. H. Lee, Y. K. Kim, C. Won, S.-H. Lee, K. P. Kim, J. Kuret, D.-H. Min, M. J. Lee, Nat. Commun. 2014, 5, 5633.

[5] H. Fan, Z. Zhao, G. Yan, X. Zhang, C. Yang, H. Meng, Z. Chen, H. Liu, W. Tan, Angew. Chem. 2015, 127, 4883.

[6] M. Kovochich, M. Liong, A. E. Nel, J. Lu, T. Xia, F. Tamanoi, J. I. Zink, S. G. Ruehm, ACS Nano 2008, 2, 889.

[7] J. Kim, H. S. Kim, N. Lee, T. Kim, H. Kim, T. Yu, I. C. Song, W. K. Moon, T. Hyeon, Angew. Chem. 2008, 120, 8566

[8] A. Kumar, Austin J. Nanomed. Nanotechnol. 2014, 2, 1017.

[9] N. J. Yang, M. J. Hinner, Methods in Molecular Biology, Springer, Berlin, Germany 2015, 42.

[10] E. Blanco, H. Shen, M. Ferrari, Nat. Biotechnol. 2015, 33, 941.

[11] L. Sercombe, T. Veerati, F. Moheimani, S. Y. Wu, A. K. Sood, S. Hua, Front. Pharmacol. 2015, 6, 286.

[12] Y. Patil, Y. Amitay, P. Ohana, H. Shmeeda, A. Gabizon, J. Controlled Release 2016, 225, 87.

[13] S. K. Sriraman, J. Pan, C. Sarisozen, E. Luther, V. Torchilin, Mol. Pharmaceutics 2016, 13, 428.

[14] J. Q. Gao, Q. Lv, L. M. Li, X. J. Tang, F. Z. Li, Y. L. Hu, M. Han, Biomaterials 2013, 34, 5628.

[15] B. Garnier, S. Tan, C. Gounou, A. R. Brisson, J. Laroche-Traineau, M. J. Jacobin-Valat, G. Clofent-Sanchez, Biointerphases, Vol. 7, Springer, Berlin, Germany 2012, 1.

[16] Y. Xiang, R. Kiseleva, V. Reukov, J. Mulligan, C. Atkinson, R. Schlosser, A. Vertegel, Langmuir 2015, 31, 12177.

[17] H. Kang, M. B. O'Donoghue, H. Liu, W. Tan, Chem. Commun. 2010, 46, 249.

[18] J. Ma, H. Zhuang, Z. Zhuang, Y. Lu, R. Xia, L. Gan, Y. Wu, Artif. Cells, Nanomed., Biotechnol. 2018, 46, 1864.

[19] J. Yang, Y. Shimada, R. C. L. Olsthoorn, B. E. Snaar-Jagalska, H. P. Spaink, A. Kros, ACS Nano 2016, 10, 7428.

[20] G. Godeau, C. Staedel, P. Barthélémy, J. Med. Chem. 2008, 51, 4374.

[21] M. E. Todhunter, N. Y. Jee, A. J. Hughes, M. C. Coyle, A. Cerchiari, J. Farlow, J. C. Garbe, M. A. LaBarge, T. A. Desai, Z. J. Gartner, Nat. Methods2015, 12, 975.

[22] M. Kwak, A. J. Musser, J. Lee, A. Herrmann, Chem. Commun. 2010, 46, 4935.

[23] E. Akbari, M. Y. Mollica, C. R. Lucas, S. M. Bushman, R. A. Patton, M. Shahhosseini, J. W. Song, C. E. Castro, Adv. Mater. 2017, 29, 1.

[24] J. Willem de Vries, S. Schnichels, J. Hurst, L. Strudel, A. Gruszka, M. Kwak, K. U. Bartz-Schmidt, M. S. Spitzer, A. Herrmann, Biomaterials 2018, 157, 98.

[25] T. Tokunaga, S. Namiki, K. Yamada, T. Imaishi, H. Nonaka, K. Hirose, S. Sando, J. Am. Chem. Soc. 2012, 134, 9561.

[26] M. You, Y. Lyu, D. Han, L. Qiu, Q. Liu, T. Chen, C. Sam Wu, L. Peng, L. Zhang, G. Bao, W. Tan, Nat. Nanotechnol. 2017, 12, 453.

[27] J. R. Burns, N. Al-Juffali, S. M. Janes, S. Howorka, Angew. Chem. 2014, 126, 12674.

[28] L. Sun, Y. Gao, Y. Wang, Q. Wei, J. Shi, N. Chen, D. Li, C. Fan, Chem. Sci. 2018, 9, 5967.

[29] J. Yang, A. Bahreman, G. Daudey, J. Bussmann, R. C. L. Olsthoorn, A. Kros, ACS Cent. Sci. 2016, 2, 621.

[30] Y. Jiang, R. Tang, B. Duncan, Z. Jiang, B. Yan, R. Mout, V. M. Rotello, Angew. Chem. 2015, 127, 516.

[31] M. Kaksonen, A. Roux, Nat. Rev. Mol. Cell Biol. 2018, 19, 313.

[32] A. L. Kiss, E. Botos, J. Cell. Mol. Med. 2009, 13, 1228.

[33] S. Mayor, R. E. Pagano, Nat. Rev. Mol. Cell Biol. 2007, 8, 603.

[34] L. Wang, K. G. Rothberg, R. G. W. Anderson, J. Cell Biol. 1993, 123, 1107.

[35] S. K. Rodal, G. Skretting, Ø. Garred, F. Vilhardt, B. Van Deurs, K. Sandvig, Mol. Biol. Cell 1999, 10, 961.

[36] P. C. Patel, D. A. Giljohann, W. L. Daniel, D. Zheng, A. E. Prigodich, C. A. Mirkin, Bioconjugate Chem. 2010, 21, 2250.

[37] C. Hang, J. Choi, L. Hao, S. P. Narayan, E. Auyeung, C. A. Mirkin, Proc. Natl. Acad. Sci. 2013, 110, 2.

[38] G. Vindigni, S. Raniolo, A. Ottaviani, M. Falconi, O. Franch, B. R. Knudsen, A. Desideri, S. Biocca, ACS Nano 2016, 10, 5971.

[39] Z. Z. Yang, J. Q. Li, Z. Z. Wang, D. W. Dong, X. R. Qi, Biomaterials 2014, 35, 5226.

[40] G. A. Daudey, H. R. Zope, J. Voskuhl, A. Kros, A. L. Boyle, Langmuir 2017, 33, 12443.

[41] S. Piao, R. K. Amaravadi, Ann. N. Y. Acad. Sci. 2016, 1371, 45.

[42] A. H. Futerman, G. Van Meer, Nat. Rev. Mol. Cell Biol. 2004, 5, 554.

[43] V. Linko, A. Ora, M. A. Kostiainen, Trends Biotechnol. 2015, 33, 586.

[44] S. Surana, A. R. Shenoy, Y. Krishnan, Nat. Nanotechnol. 2015, 10, 741.